

Entanglement, chaos and atomic Wigner function of the Dicke model.

L. Sanz

Departamento de Física, UFSCar, Caixa Postal 676, 13565-905, São Carlos, SP, Brasil

K. Furuya

*Instituto de Física ‘Gleb Wataghin’,
Universidade Estadual de Campinas UNICAMP,
Caixa Postal 6165, 13083-970, Campinas, SP, Brasil*

Abstract

We calculate the atomic (spin) Wigner function for the single mode Dicke model in the regime of large number of two-level atoms. The dynamics of this quasi-probability function on the Bloch sphere allows us to visualize the consequences of the entanglement process between the boson and the spin subsystems. Such investigation shows a distinct localization behavior of the spin state with respect to the polar and azimuthal Bloch sphere angles. A complete *breakdown of reflection symmetry* in the azimuthal angle is shown in the non-integrable case, even at short evolution times. Also, in the classically chaotic situation, the appearance of *sub-planck structures* in the Wigner function is shown, and its evolution analyzed.

I. INTRODUCTION

The Wigner function (WF)[1] has been an important tool in physics, particularly to explore the interface between classical and quantum world [2]. Furthermore, it is an useful ingredient in the theory of partial loss of coherence [3]. Recently, advances in the state reconstruction problems [4] renewed interest on the WF, particularly after the measurement of negative quasi-probabilities [5, 6] which are generally considered as signatures of non-classical states [7]. Also, quasi-probability functions are relevant for the study of entanglement process of continuous variables, as in the beam splitters [8], in order to analyze separability of two-mode Gaussian states [9, 10, 11], and in studies of teleportation of non-classical states like in Ref. [12]. Since the proposal of manifestation of chaos in the process of decoherence by Zurek and Paz [13], the WF has also been an important tool for studying this issue [14, 15].

Here, our focus is the use of the atomic Wigner function to study the ideal atom-field entanglement process. Recent experimental progress on arrays of quantum dots and Josephson junctions has raised the possibility of super-radiance, a phenomenon already known to arise in a system with N *two-level* atoms coupled to a field mode described by the Dicke model (DM) [16]. Some of the solid-state systems relevant to quantum information that can be mapped into DM are: ‘phonon cavity quantum dynamics’ [17, 18]; those with Josephson Junctions and quantum dots, with the possibility of multiqubit entanglement Dicke-like model [19]; and the proposal of ‘circuit QED’ [20], which has been constructed recently for one qubit Jaynes-Cummings case [21]. Finally, the atom-molecule coexistence model near a Feshbach resonance of cold fermions in both strong [22] and weak [23] coupling has been proposed as a DM.

We are interested in exploring the atomic (spin) Wigner function dynamics of the generalized N -Jaynes-Cummings model (N -JCM) [24] where both Jaynes-Cummings (JC) and anti-Jaynes-Cummings (AJC) interaction can be present. These interactions between spin and boson systems has been shown to appear naturally in trapped ions [25, 26], or in cavity QED by means of strong classical driving field [27]. Classically the model becomes chaotic [28, 29, 30], and some of its manifestation in the entanglement process has been shown in previous publications [31, 32, 33, 34, 35]. To our knowledge, it is the first time the dynamical evolution of the N -qubits atomic Wigner function is followed in detail during the

entanglement process since it has been introduced [36, 37, 38].

Remarkable features in the AWF can be seen in such wave-packet dynamics, showing dynamical differences between localization of the angular variables ϕ, θ on Bloch Sphere. We also explore the dynamics of the negative-valued parts of the AWF, usually considered as a hallmark of non-classicality and interference effects. Another notable aspect is the distinct time evolution of the AWF, depending on the initial positions chosen for the centers of the wave packets. Such sensitivity to initial conditions have been already noted in references [31, 32], at the level of the integrated quantities like the subsystem linear entropy or mean values, but the details of the behavior of quasi-probability functions was lacking.

This paper is organized as follows: in Sec. II we present the classical analog of the Dicke model to define and show some quantities used in the following sections. Also, we review the notion of sensitivity of the entanglement process on the initial position of the coherent packet, in both *integrable* and *chaotic* cases, already found in previous works. Sec. III is reserved to present our results for the N -qubit atomic Wigner function for some selected initial conditions and analyze its time evolution under the point of view of the entanglement process. In Sec. IV we summarize our results.

II. THE MODEL AND ENTANGLEMENT DYNAMICS WITHIN THE LARGE- N APPROXIMATION

We consider a generalized version of N -atom (qubit) Dicke model, with variable coefficient for the rotating and counter-rotating wave term. Moreover, since our aim here is to pursue the effect of the classically chaos generating term on the entanglement between the N -atom and the field, we will ignore the interaction between the atoms (qubits) and treat the atomic system as a large spin ($N = 2J$).

$$\begin{aligned} \hat{H} = & \hbar\omega_0\hat{a}^\dagger\hat{a} + \hbar\omega_a\hat{J}_z + \frac{G}{\sqrt{2J}}\left(\hat{a}\hat{J}_+ + \hat{a}^\dagger\hat{J}_-\right) + \\ & + \frac{G'}{\sqrt{2J}}\left(\hat{a}^\dagger\hat{J}_+ + \hat{a}\hat{J}_-\right). \end{aligned} \quad (1)$$

Here, ω_0 and ω_a are frequencies associated with free Hamiltonians for field and atoms respectively. G, G' are coupling constants associated with atom-field interaction within the dipole approximation. The usual Rotating Wave Approximation (RWA) is recovered by setting

$G' = 0$. The field observable are described by means of the creation and annihilation operators \hat{a} and \hat{a}^\dagger , whereas \hat{J}_z, \hat{J}_\pm are pseudo-spin operators associated to an atomic observable. This model is used to describe both, cavity QED experiments [27, 39] (with $G = G'$, but usually to an excellent approximation one can set $G' = 0$) and trapped-ion systems. In the last system, interactions with different couplings $G \neq G'$ can be generated [25, 26].

For the purpose of our study where both systems are initially pure and separable in quasi-classical states, the appropriate initial state $|w\nu\rangle$ is a product of the field and atomic coherent states defined as [36, 40, 41]:

$$\begin{aligned} |\nu\rangle &= \hat{D}(\nu) |0\rangle = e^{-\frac{|\nu|^2}{2}} e^{\nu\hat{a}^\dagger + \nu^*\hat{a}} |0\rangle \\ |w\rangle &= (1 + |w|^2)^{-J} e^{w\hat{J}_+} |J, -J\rangle. \end{aligned} \quad (2)$$

Here, $J = N/2$ and the variables w and ν can be written as a function of the classical variables in the corresponding phase spaces, (q_f, p_f) for the field, and (q_a, p_a) for the atomic degree of freedom

$$\begin{aligned} w &= \frac{p_a + iq_a}{\sqrt{4J - (p_a^2 + q_a^2)}} \\ \nu &= \frac{1}{\sqrt{2}} (p_f + iq_f) \end{aligned} \quad (3)$$

A corresponding classical Hamiltonian can be obtained by a standard procedure [42], using the above defined coherent states $\langle w\nu | \hat{H} | w\nu \rangle$ [30]

$$\begin{aligned} \mathcal{H}(q_a, p_a, q_f, p_f) &= \frac{\omega_0}{2} (p_f^2 + q_f^2) + \frac{\omega_a}{2} (p_a^2 + q_a^2) \\ &- \omega_a J + \frac{\sqrt{4J - (p_f^2 + q_f^2)}}{4J} (G_+ p_a p_f + G_- q_a q_f), \end{aligned} \quad (4)$$

with $G_\pm = G \pm G'$. The classical dynamics associated with this Hamiltonian were explored before [30], and shown that: (i) integrable situations are recovered when either G or G' is zero; (ii) the most chaotic dynamics is associated with the condition $G = G' \approx \mathcal{O}(\omega_0, \omega_a)$, as we increase the coupling constant. Our aim is to investigate the time evolution of the initially quasi-classical wave-packet along with the occurrence of entanglement between the N -atom and the field systems. Particularly, we are looking for the possible differences in the reduced wave-packet dynamics when we compare *integrable* and *chaos generating* interactions. The connection with the classical dynamics is established by choosing coherent states as initial

states, centered at the corresponding points of the phase space. Then, we let the system evolve by means of the Hamiltonian (1) and explore the entanglement dynamics solving numerically the Schrödinger equation.

In order to know where to put the initial atomic and field wave-packets, the first step is study the structure of classical phase space. This can be done by using the Poincaré section. In Fig. 1, we plot the projection of Poincaré section in the atomic plane (q_a, p_a) for $q_f = 0$ and $p_f > 0$. The surfaces of section correspond to both, the right one to the integrable case with $(G = 0.5, G' = 0)$ and the left one to the soft chaos $(G = 0.5, G' = 0.2)$. Here, and along the present work, the total energy is fixed at $E = 2J = 21.0$ with $J = 10.5$. The coupling values corresponds to the non-super-radiant phase ($G_+ < 1$) [43]. The limit of atomic phase space is indicated by a border at radius equal to $\sqrt{4J}$. Integrable section shows a separatrix of motion along the line $p_a = 0.0$ and concentric tori around each of the two stable periodic orbits. A pro-eminent feature of the non-integrable surface of section is a large stability island for $p_a > 0$.

The symbols in Fig. 1 show the chosen centers for the atomic coherent states. We choose two specific initial conditions (i.c.) for each case. In the integrable case, the first one (I1) is on an internal tori belonging to the region $p_a > 0$, marked by a triangle; and the second (I2), marked by a circle, located near the border of the atomic phase space. For soft chaos situation, the first i.c. (N1) where chosen on a point inside the largest stability island (circle). The second condition (N2) is located in the chaotic sea (triangle). Specific values of q_a , p_a and the mean value of \hat{J}_z operator for the associated atomic coherent state are listed in Table II.

I.C.	$q_a/\sqrt{4J}$	$p_a/\sqrt{4J}$	$\langle \hat{J}_z \rangle / J$
I1	0.0	0.55	-0.43
I2	0.1	0.95	0.83
N1	0.0	0.54	-0.47
N2	0.0	-0.28	-0.84

TABLE I: q_a , p_a and $\langle \hat{J}_z \rangle$ values for the chosen initial conditions.

As a second step, one should calculate the time evolution of the atomic linear entropy (ALE) which, in this globally pure bipartite system, can be used as a measure of entangle-



FIG. 1: Poincaré section for the atomic degree of freedom (with $q_f = 0.0$ and $p_f > 0$) in the resonant case $\omega_a = \omega_0$ and energy $E = 21.$, with $N = 2J = 21$. Left: integrable case with $G = 0.5$ and $G' = 0.0$. Right: non-integrable case with $G = 0.5$ and $G' = 0.2$.

ment. This calculation is done in three stages: First we diagonalize the Hamiltonian (1) numerically and use the eigenvalues and eigenstates in order to find the temporal total density operator, $\hat{\rho}(t)$. Then, we calculate the reduced density operator of the atomic subsystem, $\hat{\rho}_a = \text{Tr}_f[\hat{\rho}(t)]$, and finally obtain $\delta_a(t) = 1 - \text{Tr}_a[\hat{\rho}_a^2(t)]$. Evolution in time of the ALE for i.c.'s I1 and I2 are plotted in Figure 2(a). For both i.c.'s, the subsystem entropy increases in the mean as time goes on, until a plateau is reached. The details of the curve such as the specific values of the ALE in the plateau, the particular oscillatory behavior and the entanglement rate depend on each initial condition. In particular, we observe that those atomic i.c.'s with the classical dynamics restricted to a well delimited region in phase space on the tori region are more resistant to entangle with field. This relation between fast entanglement process and less localized classical dynamics was pointed out in a previous work [32].

The ALE for the soft chaos situation are plotted in Fig. 2(b). In this plot, it is clear that larger entanglement rate is also associated to the chaotic i.c.'s. It is interesting to compare our results for I1 and N1, solid lines in Fig. 2(a,b). For I1, ALE shows more regularity in the oscillations and reaches the corresponding plateau around $t \approx 30$, whereas in ALE for N1 the oscillations are less regular and takes a longer time to reach the plateau, at $t \approx 70$. Also, ALE for N1 condition keeps a small oscillation around its mean value (due to the non-RWA term) and one can also see a certain large period modulation in contrast to I1. The relation between the behavior of the classical trajectory and maxima and minima of δ_a was studied in Ref. [33], and we will not discuss here. Instead, the atomic Wigner Function (AWF) is used to visualize the behavior of global state as projected in atomic phase space. In the next section, we will illustrate the following aspects: (i) that the AWF provide us the information that those i.c.'s that are more “protected” against entanglement process,

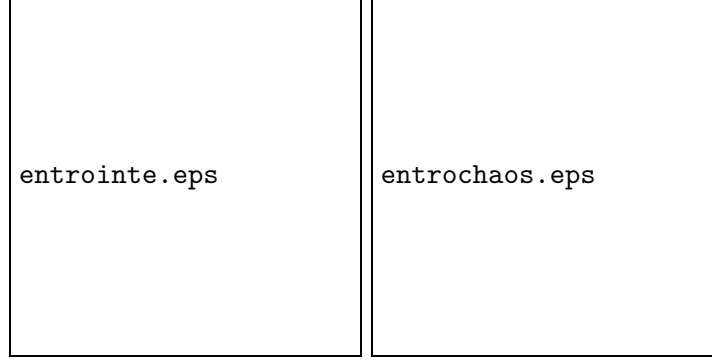


FIG. 2: Atomic Linear Entropy of the N -JCM associated with the four initial conditions centered at the positions shown in Fig. 1 (with the same parameter values) and listed in Table II. (a) Integrable case: i.c. I1 (Solid line) and I2 (dotted line); (b) Soft chaos: i.c N1 (Solid line) and N2 (dotted line).

have a strong localization on the Bloch sphere; (ii) we also show how the destruction of tori due to chaos in the classical dynamics goes along with the delocalization of the quantum wave-packet during its temporal evolution.

III. DYNAMICS OF ATOMIC WIGNER FUNCTION.

The phase space quasi-probability distributions of electromagnetic field and atom have been discussed by several authors [1, 36, 37, 44, 45]. Here, we adopt the definition of Wigner function in terms of arbitrary angular momentum basis, as introduced by Agarwal [37]. This function is defined as

$$W(\theta, \phi, t) = \sqrt{\frac{2J+1}{4\pi}} \sum_{K=0}^{2J} \sum_{Q=-K}^K \varrho_{KQ}(t) Y_{KQ}(\theta, \phi), \quad (5)$$

where $\varrho_{K,Q}$ is given by

$$\varrho_{K,Q}(t) = \text{Tr} [\rho_a(t) \hat{T}_{KQ}]. \quad (6)$$

This is the characteristic function associated with atomic density operator $\rho_a(t)$. Here, \hat{T}_{KQ} is the multipole operator acting in the angular momentum space [46]

$$\begin{aligned} \hat{T}_{KQ} = & \sum_{M=-J}^J (-1)^{J-M} \sqrt{2K+1} \begin{pmatrix} J & K & J \\ -M & Q & M-Q \end{pmatrix} \\ & \times |J, M\rangle \langle J, M-Q|. \end{aligned} \quad (7)$$

In Eq.(5), the usual Wigner $3J$ symbol has been used, and $Y_{KQ}(\theta, \phi)$ indicates the spherical harmonics defined over the Bloch sphere. There, θ is the polar angle and ϕ is the azimuthal angle. The distribution of any angular momentum state can be studied using the AWF. As shown in Dowling *et al.* [38], it is possible to estimate the indeterminacy in the measure of the atomic observable $\hat{J}_z, \hat{J}_x, \hat{J}_y$ in the state through its variances. In fact, if the state has a large probability associated to a well-defined eigenvalue of \hat{J}_z , its atomic Wigner function shows a strong localization in polar angle θ . In a similar way, indeterminacy associated to the measure of \hat{J}_x and \hat{J}_y means ignorance on the azimuthal angle ϕ .

In order to obtain the AWF, we use our previous results of atomic density matrix operator. Because the basis used was the Dicke states $|\hat{J}, \hat{J}_z\rangle$, we can calculate the action of \hat{T}_{KQ} on each atomic density matrix elements, obtaining $W(\theta, \phi, t)$. Also, we always set the $\phi = 0$ value exactly at the center of each initial atomic coherent packet. That means, if the wave packet is not on the X -axis, we rotate the XY plane by a certain angle $\phi(t = 0) = \phi_0$ in such a way that the direction defined by the vector $(\sin \phi_0, -\cos \phi_0, 0)$ coincides with the rotated X -axis.

A. Integrable case with $G = 0.5$ and $G' = 0$.

For the integrable case, we show the snapshots of the temporal evolution of contour lines of AWF in Fig. 3 for the i.c. I1. The initial coherent state, Fig. 3(a), has its maximum value (3.5) at $\theta = 0.64\pi$, which corresponds to $\langle \hat{J}_z \rangle \approx -0.43J$. At the time when the first maxima of ALE is reached, the atomic state has a more delocalized distribution, shown in Fig. 3(b), with two negative valued regions (in black). A formation of three overlapping positive peaks starts, with maxima (almost) at the equator of Bloch sphere ($\theta = \pi/2$). At this time, AWF has a maximum value lower than the one at the initial time (≈ 1.7). The appearance of a negative part in the AWF with value ≈ -0.2 (10% of maximum value) indicates the non-classical character of this state.

The delocalization of the state in the azimuthal angle is associated with the increase of the ALE. This assertion can be confirmed by checking the evolution for consecutive maxima and minima. The forms of AWF are shown at times corresponding to the *first minimum*, Fig. 3(c); *second maximum*, Fig. 3(d), and *second minimum*, Fig. 3(e). Comparing them, it is clear that the AWF is more localized in the ϕ variable at times when ALE has minima.

Although in Fig. 3(d), the three peaks have coalesced into one, the packet sweeps a larger interval over ϕ values than those found at the first minimum time scale. We can also observe that AWF maximum value oscillates around $\theta \approx 1.8$. A negative valued portion is still present but it became significantly smaller (less than 1%) than in Fig 3(b), so it is not possible to see in Fig 3(c,d), but reappears in Fig. 3(e). From this sequence, it is clear that atomic state loses both, azimuthal and polar localization, associated with the increase in the atomic linear entropy. However, at those times when the ALE plateau is reached, we see how the AWF (plotted in dotted lines) still has localization in θ (near the equator in the Bloch sphere), having non-zero values only in the interval $1.6 \leq \theta \leq 2.5$. This shows that for the particular initial condition considered on an internal torus (distant from the separatrix motion and the border of the phase space), an increase in the ALE is associated with the increasing delocalization with respect to the azimuthal angle much more than to the polar variable.

Now we shall compare previous case with the time evolution of the AWF for condition I2 ($\theta \approx 0$) which is close to the largest value of $\langle \hat{J}_z \rangle$, shown in Fig. 4. At the initial time, Fig. 4(a), the AWF is well localized in both angular variables and, as the two subsystems interact, we can see that the AWF begins to lose localization mostly in the polar variable (non-zero values in the interval $1.0 \leq \theta \leq 2.7$), at the time scale of the first maximum in ALE. Physically, the spreading of the AWF and the increase in the atomic linear entropy, tell us that for this i.c. (I2), the increasing entanglement of the N -atoms with the field is mostly associated with an increase of the participating states of atomic levels in the \hat{J}_z spectrum (shown by the spreading of the AWF in θ variable). The value of the ALE at the first maximum for I2 ($\delta_a \approx 0.5$) is greater than for I1 (δ_a lower than 0.2), where the increasing delocalization is primarily in the azimuthal variable ϕ .

At the time corresponding to the *first minimum* of the ALE, Fig. 4(c), we observe that AWF forms a three-peak structure seen in the I1 case. However, there is a appreciable spreading in the ϕ variable but not allowing the peaks to become separated, and near the central position in $\phi = 0$ occurs also a notable delocalization in θ variable. The negative part is no longer localized as in the previous i.c., and its value is $\approx 10\%$ of the maximum of AWF. Again, we observe the connection between minima of δ_a and the angular localization: the AWF for the second maximum of ALE, Fig. 4(d), shows how the atomic state is completely delocalized in both variables at this time. The AWF is non-zero practically at all points

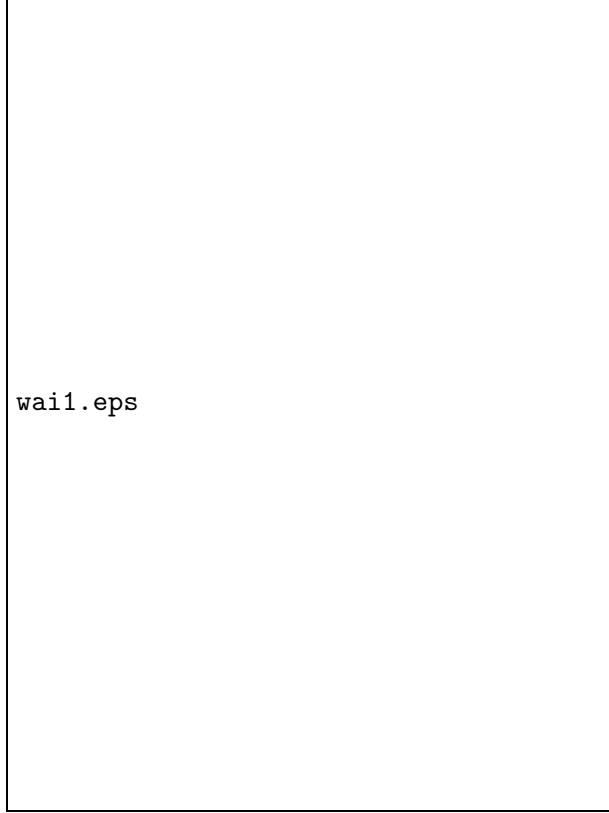


FIG. 3: Shaded contour plots of atomic Wigner function associated with the i.c. I1: (a) initial time; (b) *first maxima* of the corresponding atomic linear entropy (ALE); (c) *first minimum* of ALE; (d) *second maxima*; (e) *second minima*; (f) $t = 40$ at the *plateau region*. Negative valued regions of AWF are drawn in black.

on the atomic phase space. This situation is reversed at the time of the second minimum of ALE, with a tentative to re-gain some localization in θ variable and a structure which roughly resembles Fig. 4(b). It is also interesting to see how the negative part of AWF reappears and it is even more pronounced than in the previously referred time ($\approx 20\%$). At times when the plateau is reached the AWF is totally delocalized and not even a signal of a main positive peak is present, which was the case we found in the plateau times of the internal torus case. Negative part is less than 1% of maximum value of AWF.

From this results, it is clear that initial condition I1 dynamically preserves the localization of the AWF, especially in the polar angle. This is associated with a certain *inhibition in the entanglement process*. The difference on the value of the atomic linear entropy between the two initial conditions presented here is clearly related with the delocalization process in both

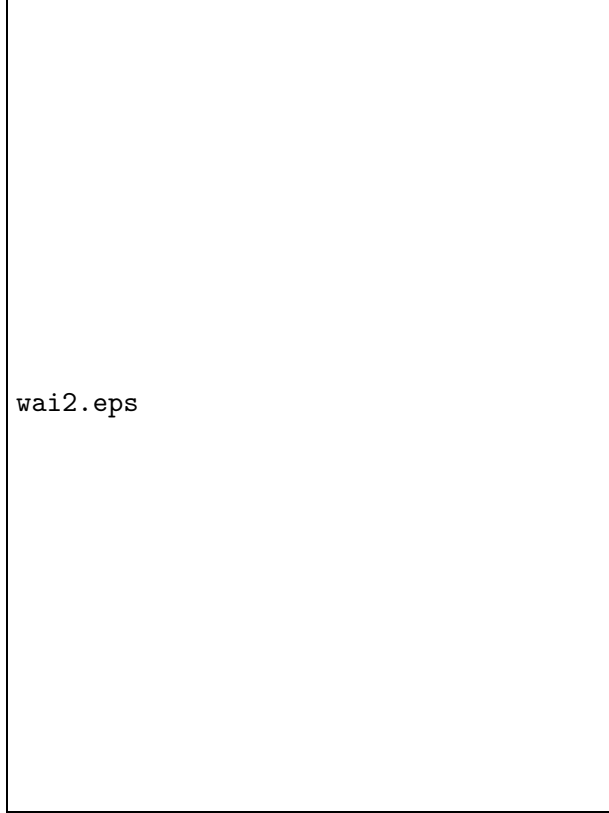


FIG. 4: Shaded contour plot atomic Wigner function associated with the i.c. I2: (a) initial time; (b) *first maxima* of corresponding atomic linear entropy (ALE); (c) *first minimum* of ALE; (d) *second maxima*; (e) *second minima*; (f) $t = 40$ at the *plateau region*. Negative valued regions of AWF are drawn in black.

azimuthal and polar angles. Hence, the dynamics of the internal tori is protected against the entropy increase, and this is related with the localization in the polar angle; whereas, the i.c.'s located near the separatrix and the border do not have such a dynamical protection. Other initial coherent states with similar characteristics has qualitatively analogous behavior for the ALE.

Another characteristic is the clear appearance of some *sub-planck structures*, namely the structures with considerable amplitudes with their supports in areas much smaller than \hbar in phase space, similar to those discussed by Zurek [15]. On the Bloch sphere, the minimum action area (\hbar is taken to be 1 here) is associated with the size of atomic coherent state (at $t = 0$) which defines a minimum-uncertainty packet. This minimum action area can be inferred, for instance, in Fig. 3(a) and Fig. 4(a) for $N=21$. Such sub-planck structures which

are peaks confined in areas significantly smaller than the size of the initial packet in the (ϕ, θ) -plane appear for instance in Figs 4(f), 5(d,f) and 6(f). It is interesting to note that its appearance is indeed connected with the time where the atomic subsystem has lost its own coherence by entangling with the field. What is remarkable is that, for the integrable case, the entanglement process leaves the AWF with sub-planck structure *only* for i.c. I2 but not for I1. This is, to one side, AWF counterpart of the *rapid loss of coherence* that occurs for the wave packet located near the separatrix of motion [32], but it is more than simply accelerating the entanglement process: the dynamical instability also generates structures similar to chaotic case as we shall see in the next subsection.

B. Non-integrable case: $G = 0.5$ and $G' = 0.2$

Now, we present in Figures 5-6 our results for the time evolution of the AWF corresponding to the *non-integrable* case for the conditions N1 (regular region) and N2 (chaotic region). Some similarities between integrable and non-integrable cases can be noticed: first, the connection between oscillatory behavior and a delocalization-localization of AWF are still present even in the chaotic i.c. (N2). This can be seen, for example, in Figs. 6(c, e), as compared with Fig. 6(d). There, AWF seems to suffer a “recoil” to a restricted area in (ϕ, θ) plane at times which correspond to a minimum in the ALE (corresponding to the behavior of Figs. 4(c, e) compared with Fig. 4(d) of the integrable case). Second feature is related with the similar “tori protection” that was found in the integrable case. Comparing the forms of AWF in the plateau region, Fig. 5(f) and Fig. 6(f), a more localized AWF (particularly for the positive-valued part) is evident for the first condition (N1) inside the large stability island than the second one (N2) in the chaotic region. Notice that, we also obtain a certain difference for the ALE plateau values in Fig. 2(b).

The most interesting aspects are the dynamical differences between the two cases. Notice that, in the *integrable* case, AWF has an azimuthal mirror symmetry: $\phi \rightarrow -\phi$, the $\phi < 0$ region being a mirror image of the $\phi > 0$ region. This symmetry is not present in the *non-integrable* case. At this point, it is important to recall that this symmetry breaking is already observed in the classical Poincaré section in atomic phase space (see Fig. 1). Since we are studying a situation within the large- N limit, this symmetry breaking can be associated with *quantum chaos* at the level of spectral distribution [29]. Another distinguishable feature is

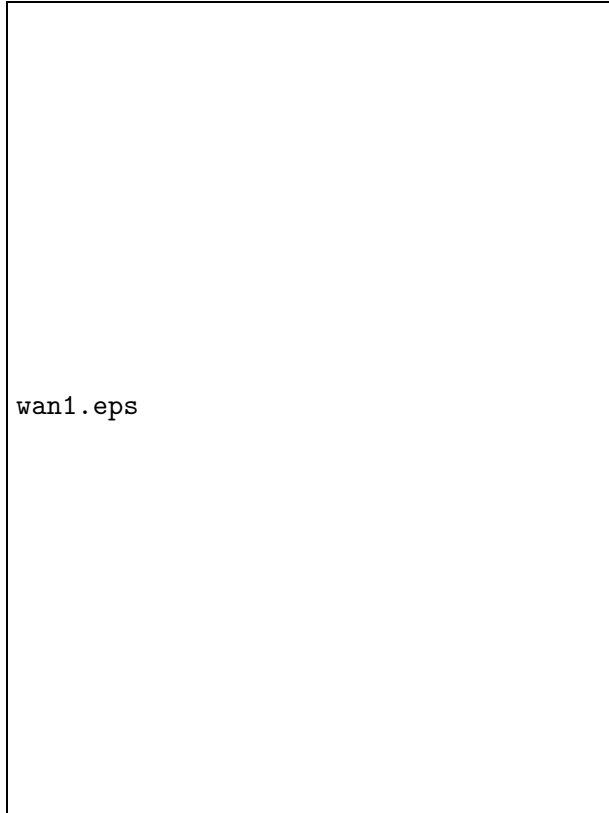


FIG. 5: Shaded contour plot of the atomic Wigner function associated with i.c. N1: (a) initial time; (b) *first maxima* of corresponding atomic linear entropy (ALE); (c) *first minimum* of ALE; (d) *second minimum*; (e) *third maxima*; (f) $t = 70$ at the *plateau region*. Negative valued regions of AWF are drawn in black.

the behavior of the sub-planck structures in the AWF. They have appeared in Fig. 5(b), in spite of the tori protection, and remain for times at the plateau region. The size of this sub-planck structures seems to saturate after the entanglement time, confirming for the present model the results shown by Zurek. Also, it is notable the presence of a larger number of negative sub-planck packets than positive ones, although we do not have any explanation for this fact.

IV. SUMMARY

This work gives a complete analysis of the temporal behavior of the entanglement process in the N -JCM in the large- N wave packet dynamics. Previous results have pointed out the sensitivity to initial conditions of the atomic linear entropy. Here, a calculation of the atomic

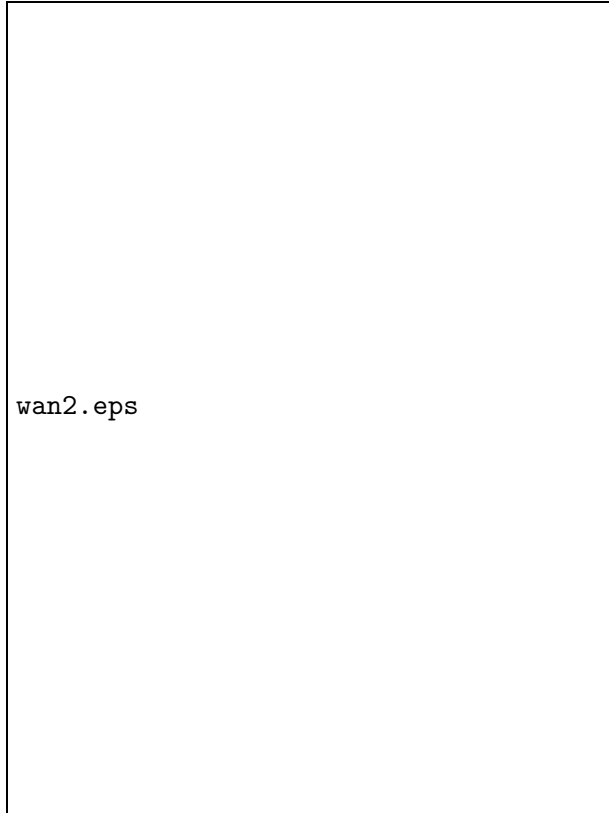


FIG. 6: Shaded contour plot of the atomic Wigner function associated with i.c. N2: (a) initial time; (b) *first maxima* of the corresponding atomic linear entropy (ALE); (c) *first minimum* of the ALE; (d) *second maxima*; (e) *second minima*; (f) $t = 70$ at the *plateau region*. Negative valued regions of AWF are drawn in black.

Wigner function allowed us to uncover additional information about the atomic subsystem, not visible in an integrated quantities like the entropy. This allowed us to have a better idea of what is happening to the reduced atomic state during the entanglement process, as a function of both, the type of interactions present (rotating and counter-rotating) and the initial position of the coherent wave-packet.

A very conspicuous information obtained in this way, is the dynamics of the amount of the delocalization of the AWF during the entanglement process as a function of both angular variables on the Bloch sphere. Also, we show that the presence of the classical tori structure in the phase space surrounding the center of the coherent wave packet, is an indication at the quantum level of a certain inhibition in the coherence loss. Thus, by breaking the integrability we also break this protection against delocalization in the polar angle for the

initial coherent state centered on the internal tori. However, the regular surrounding is still an indication of slower loss of coherence and, apparently the larger the island of stability around the wave packet, stronger is this effect on the quantum wave packet. The symmetry breaking of the AWF for any time ($t > 0$) is another characteristic of the non-integrable case.

The most interesting aspect is the dynamics of the sub-planck structures: it is completely absent in the regular initial conditions of the integrable situation, but do appear in the long-time (ALE plateau region) behavior for the packet placed near the separatrix of motion. In the non-integrable case, even the wave packets placed inside the regular island do develop sub-planck structures well before the plateau of the ALE is reached, and the chaotic cases show such structures already at the first maximum of the ALE. Such sub-planck structures seems to be directly associated with the destruction of the “tori protection” and faster entanglement due to less restricted dynamics in phase space, thus being an indicator of dynamical instability connected to *quantum chaos*.

Acknowledgments

It is a pleasure to acknowledge R. M. Angelo for many helpful discussions. We thank financial support from FAPESP (Fundação de Amparo à pesquisa do Estado de São Paulo) under grant 03/06307-9 and CNPq (Conselho Nacional de Pesquisa, Brazil) under grants 146010/99-0 and 300651/85-6.

-
- [1] E.P. Wigner, Phys. Rev. **40**, 749 (1932); M. Hillery et al., Phys. Rep. **106**, 121 (1997).
 - [2] V.M. Berry in *Chaotic Behaviour of Deterministic Systems*, Les Houches XXXVI, ed. by Iooss et. al (North-Holland, Amsterdam, 1983);
 - [3] W.H. Zurek, Rev. Mod. Phys. **75**, 715 (2003); **outros**.
 - [4] see review by D.-W. Welsch and V. Vogel in *Progress in Optics XXXIX*, ed. by E. Wolf (North Holland, Amsterdam, 1999) p.65.
 - [5] D. Leibfried et al., Phys. Rev. Lett. **77**, 4281 (1996).
 - [6] P. Bertet et al. Phys. Rev. Lett. **89**, 200402(2002).
 - [7] D. Leibfried, T. Pfau and C. Monroe, Phys. Today **22** (1998).

- [8] M.S. Kim, W. Son, V. Buzek and P.L. Knight, Phys. Rev. A **65**, 032323 (2002).
- [9] L.-M. Duan et al Phys. Rev. Lett. **84**, 2722 (2000).
- [10] R. Simon, Phys. Rev. Lett. **84**, 2726 (2000).
- [11] P. Marian et al. J. Phys. A, **34**, 6969 (2001).
- [12] J. Lee, M. S. Kim and H. Jeong, Phys. Rev. A **62**, 032305 (2000).
- [13] W. H. Zurek and J. P. Paz, Physica (Amsterdam) D **83**, 300 (1995).
- [14] S. Habib, K. Shizume and W. H. Zurek, Phys. Rev. Lett. **80**, 4361(1998).
- [15] W.H. Zurek, Nature **412**, 712 (2001).
- [16] R.H. Dicke, Phys. Rev. **93**, 99 (1954); see also M. Tavis and F.W. Cummings, Phys. Rev. **170**, 379 (1968).
- [17] E.M. Weig *et al*, Phys. Rev. Lett. **92**, 046804 (2004).
- [18] T. Vorrath and T. Brandes, Phys. Rev. B **68**, 035309 (2003).
- [19] C.H. Lee and N.F. Johnson, Phys. Rev. Lett. **93**, 83001 (2004).
- [20] A. Blais *et al.*, Phys. Rev. A **69**, 062320 (2004).
- [21] A. Wallraff *et al.*, Nature **431** 162 (2004).
- [22] R.A. Barankov and L.S. Levitov, Phys. Rev. Lett. **93**, 04130403 (2004).
- [23] V.A. Andreev, V. Gurarie and L. Radzihovsky, Phys. Rev. Lett. **93**, 04130402 (2004).
- [24] E. T. Jaynes and F. W. Cummings, Proc. IEEE **51**, 89 (1963); B. W. Shore and P. L. Knight, J. Mod. Opt. **40**, 1195 (1993).
- [25] J. I. Cirac, A. S. Parkins, R. Blatt, and P. Zoller, Adv. At. Mol. Opt. Phys. **37**, 237 (1996).
- [26] E. Solano, R.L. de Matos Filho and N. Zagury, Phys. Rev. Lett. **87**, 060402 (2001).
- [27] E. Solano, G.S. Agarwal and H. Walther, Phys. Rev. Lett. **90**, 027903 (2003).
- [28] P. W. Milonni, J. R. Akerhalt, and H. W. Galbraith, Phys. Rev. Lett. **50**, 966 (1983); R. Graham and M. Hönerbach, Z. Phys. B **57**,233 (1984).
- [29] C.H. Lewenkopf, M.C. Nemes, V. Marvulle, M.P. Pato, and W.F. Wreszinski, Phys. Lett. A **155**, 113 (1991).
- [30] M.A.M de Aguiar, K. Furuya, C.H. Lewenkopf, and M.C. Nemes, Ann. Phys. **216**, 291 (1992); *ibidem*, Europhys. Lett. **15**, 125 (1991).
- [31] K. Furuya, M.C. Nemes, and G.Q. Pellegrino, Phys. Rev. Lett **80** 5524 (1998).
- [32] R. M. Angelo, K. Furuya, M. C. Nemes, and G. Q. Pellegrino, Phys. Rev. A **60**, 5407 (1999).
- [33] R. M. Angelo, K. Furuya, M. C. Nemes, and G. Q. Pellegrino, Phys. Rev. A **64**, 43801 (2001).

- [34] C. Emary and T. Brandes, Phys. Rev. Lett. **90**, 044101 (2003); Phys. Rev. A **69**, 42110 (2004); Phys. Rev. E **67**, 066203 (2003).
- [35] X.-W. Hou and B. Hu, Phys. Rev. A **69**, 042110 (2004).
- [36] F. T. Arecchi, E. Courtens, R. Gilmore, and H. Thomas, Phys. Rev. A **6**, 2211 (1972).
- [37] G. S. Agarwal, Phys. Rev. A **24**, 2889 (1981).
- [38] J. P. Dowling, G. S. Agarwal, and W. P. Schleich, Phys. Rev. A **49**, 4101 (1994).
- [39] L. Davidovich, A. Maali, M. Brune, J. M. Raimond, and S. Haroche, Phys. Rev. Lett. **71**, 2360 (1993).
- [40] R. J. Glauber, Phys. Rev. **131**, 2766 (1963).
- [41] W. -M. Zhang, D. H. Feng, and R. Gilmore, Rev. Mod. Phys. **62**, 867 (1990).
- [42] P. Kramer and M. Saraceno, *Geometry of the Time-Dependent Variational Principle in Quantum Mechanics*, Lecture Notes in Physics **140** (Springer-Verlag, New York, 1981).
- [43] M.A.M. de Aguiar, K. Furuya and M.C. Nemes, Quantum Optics,**3**, 305-314 (1991).
- [44] C. C. Gerry and P. Knight, Am. J. Phys. **65**, 964 (1997).
- [45] R. L. Stratonovich, Sov. Phys. JETP **4**, 891 (1957).
- [46] R. N. Zare, *Angular Momentum.*, Baker lecture series (John Wiley & Sons, 1988), chap 2 and 5.

